Data-driven LPV Control for Micro-disturbance Rejection in a Hybrid Isolation Platform

Elias Klauser, and Alireza Karimi

***Abstract*—A novel approach for linear parameter-varying (LPV) controller synthesis for adaptive rejection of time-varying sinusoidal disturbances is proposed. Only the frequency response data of a linear time-invariant (LTI) multiple-input multiple-output (MIMO) system is used to design the LPV controller that stabilizes the system for arbitrary fast variation of the scheduling parameter. Global stability is achieved thanks to the specific structure of the LPV controller and the use of integral quadratic constraints (IQC) to represent the variation of the scheduling parameter. The LPV controller is designed by convex optimization in the frequency domain. For experimental validation of the proposed method, a hybrid micro-vibration damping platform for space applications is considered. An LPV controller for rejection of unknown time-varying disturbances is designed and implemented on the real system. Experimental results show the effectiveness of the proposed approach for rejection of disturbances and closed-loop stability for arbitrarily fast time-varying scheduling signals.**

***Index Terms*—Data-driven control, Adaptive control, Linear parameter-varying systems, Convex optimization, Frequency-domain identification for control.**

I. Introduction

Disturbance rejection is a very important task in control design as noise or external perturbations can significantly degrade the control performance. Numerous applications such as active suspension systems [1], optical stabilisation [2], control of robotic systems [3], vibration suppression in machinery [4] and active noise cancelling systems [5], [6] rely on an effective disturbance rejection control. Oftentimes, the perturbation signals in such systems are periodic and can be represented as a sum of sinusoidal signals.

In such cases when the disturbance model is known a priori, control design based on the internal model principle (IMP) can be applied. An adaptive IMP- and model-based control design can be implemented using an observer to estimate the states of the disturbance model. These estimated states can then be used to adaptively reject a harmonic disturbance [7], [8]. Alternatively, the disturbance can be modeled as a linear parameter-varying (LPV) system in a linear fractional representation (LFR) [6]. The time-varying disturbance characteristics are captured by the scheduling parameter of the LPV model while the same scheduling parameter is used for the adaptation of an LPV controller. A collection of different approaches to a benchmark on adaptive rejection of unknown and time-varying multiple narrow band disturbances can be found in [9]. An active suspension system composed of a passive damper, an inertial actuator, a shaker, a transducer and an integrated controller is used for the study. The goal is to achieve rejection of multiple narrow-band sinusoidal disturbances without measuring them by using a feedback approach. As the disturbance signal is unknown, it must be estimated for controller adaptation. The authors in [10] propose an inversed plant model approximation. The compensation signal is generated by applying the estimated disturbance signal to the inverse plant model. An indirect adaptation approach is presented in [11] where a fixed-order H_∞ gain-scheduled controller is designed using convex optimization methods. This LPV controller, designed based on frequency-domain data, uses the estimated disturbance harmonics as scheduling signals for disturbance rejection. The case of adaptive unknown narrow-band rejection in presence of uncertain plants is treated in [12]. A dual Youla-Kuçera parametrization is used to incorporate the description of the plant model uncertainties by expressing a relation between the nominal and the uncertain plant. These model-based approaches require the availability of an accurate parametric plant model which must otherwise be identified. This system identification step can be very time-consuming and therefore costly, especially for complex systems. It is estimated that around 75% of the development cost for an advanced control system go into mathematical modelling [13].

For that reason, data-driven control design techniques are becoming increasingly attractive for industrial applications thanks to recent technological developments leading to higher computational power and improved sensor technologies. These techniques can directly minimise a control criterion based on measured input-output data, making them particularly advantageous in cases where a parametric plant model is unavailable or is difficult to identify. Frequency response data can effectively be used for the analysis and synthesis of linear control systems, as it can be easily computed from input-output data avoiding any modelling error. Such methods are widely used in industry as examplified by the classic loop shaping technique. As most control performance and robust stability conditions can be represented in the frequency domain, new data-driven methods that employ only frequency-domain data and convex optimisation programming to compute robust controllers have been proposed in the literature. A fixed-structure data-driven controller design method for multivariable systems with mixed $\mathcal{H}_2/\mathcal{H}_\infty$ sensitivity performance is proposed in [14] and applied to passivity-based controller design [15] and the distributed control of microgrids [16]. This approach can be

*This work is funded by the European Space Agency ESA Contract No. 4000133258/20/NL/MH/hm.

E. Klauser is with CSEM SA, Rue Jaquet-Droz 1, CH-2002 Neuchâtel, Switzerland, and also with the Laboratoire d'Automatique, École Polytechnique Fédérale de Lausanne, CH-1015 Lausanne, Switzerland (e-mail: elias.klauser@csem.ch)

A. Karimi is with the Laboratoire d'Automatique, École Polytechnique Fédérale de Lausanne, CH-1015 Lausanne, Switzerland (e-mail: alireza.karimi@epfl.ch)

extended to linear parameter-varying (LPV) control design applying a gridding to the scheduling parameter vector using a fixed number of operating points [17]. A simlilar approach was applied to a Cartesian robot with nonlinear dynamics for position-dependent control in [18]. A frequency-domain gain-scheduled control design for rejection of time-varying narrow-band disturbances is presented in [11]. All those methods consider control design constraints at frozen operating points and do not strictly guarantee stability for the time-varying nature of the scheduling parameters. Intrinsic stability guarantees for the arbitrarily fast variation of scheduling parameters have been proposed for model-based approaches [6] and are missing in the state of the art of data-driven methods.

The Integral Quadratic Constraints (IQC) framework, introduced in [19], provides a flexible mathematical approach for representation and analysis of various forms of nonlinearities and uncertainties, including parametric uncertainties, rate-bounded uncertainties, time-delays, and norm and sector bounded nonlinearities. This framework can be used to establish sufficient stability conditions in frequency-domain and to analyse systems with multiple uncertainty types using a single composite IQC. Various techniques have been developed for model based robust control analysis and synthesis using IQC framework [20], [21], including a MATLAB toolbox [22]. However, in the data-driven context, there are limited results. A necessary and sufficient condition has been developed for linear time-invariant (LTI) system to satisfy a given IQC using single input–output trajectory of finite length [23]. Data-driven methods that combine robust stability and performance analysis in an IQC-based optimisation have been explored for designing MIMO linear parameter-varying (LPV) controllers directly from frequency-domain data [24]. This method is employed for LPV controller design of control moment gyroscopes (CMG) in [25]. Note again that all the presented LPV control design approaches provide only local stability guarantees for frozen dynamics at selected operating points. Stability guarantees for the variation of the scheduling parameter are not strictly provided.

In this paper, the objective is to synthesize a control system that can effectively reject unknown time-varying sinusoidal disturbances while ensuring closed-loop stability. This is achieved using only the frequency-domain data obtained from the LTI plant model and no parametric model is required. The control system consists of three main components: an online disturbance frequency estimator, an LPV controller with a scheduling parameter as a function of the estimated disturbance frequency, and an LTI controller. The LPV controller is an inverted notch filter with a variable center frequency, obtained from the frequency estimator, to asymptotically reject time-varying disturbances. Meanwhile, the LTI controller is designed to guarantee closed-loop stability, even in the presence of rapid variations in the estimated frequency within the LPV controller, while achieving the desired performance. The main idea is to augment the LTI plant model with the LPV controller in the frequency domain, and pull out the scheduling parameter as a time-varying uncertainty. Then, the IQC formalism is used to compute an LTI controller for the augmented LPV plant that stabilizes the closed-loop system for the arbitrary fast variation of the scheduling parameter. A novel linear matrix inequality (LMI) based on the IQC framework is presented allowing to guarantee stability for a bounded interval of the scheduling parameter. In addition, a significant reduction of computational complexity over current methods is achieved as no gridding of the scheduling parameter vector is required.

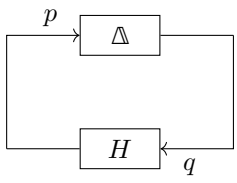

Fig. 1. Basic feedback configuration

The remainder of the paper is organised as follows: First, the notations, the basic problem, the IQC formalism and a general frequency-domain control synthesis for LFT systems are introduced (Section II). Then, a two-step iterative LPV control design algorithm for single- and multi-harmonic rejection is presented using an IQC-based LMI constraint (Section III). The resulting controller guarantees stability for arbitrarily fast time-varying scheduling parameters lying in a bounded interval. Finally, the proposed method is used to design an adaptive control scheme for a hybrid active-passive micro-vibration damping platform (MIVIDA) with the goal of adaptively rejecting unknown external perturbations (Section IV). The MIVIDA is a demonstrator for a spaceborne system that was designed to actively isolate a sensitive payload from vibrations present on board of the spacecraft.

II. Preliminaries

Notations:: The set of real rational stable transfer functions with bounded infinity norm is denoted by $\mathcal{RH}_\infty$. $A \succ (\succeq)\, B$ indicates that $A - B$ is a positive (semi-) definite matrix and $A \prec (\preceq)\, B$ indicates $A - B$ is negative (semi-) definite. The zero and identity matrices of appropriate size are denoted $\mathbf{0}$ and I respectively. The transpose of a matrix A is denoted by A^T and its conjugate transpose by A^*. Right inverse of A is denoted as $A^R := A^*(AA^*)^{-1}$, and its left inverse is denoted as $A^L := (A^*A)^{-1}A^*$. For continuous-time systems $\Omega := \mathbb{R}$ and for discrete-time systems $\Omega := [-\pi/T_s, \pi/T_s)$, where T_s is the sampling time.

A. Integral Quadratic Constraints

Two signals p and q are said to satisfy the IQC defined by a multiplier Π, if

$$\int_\Omega \begin{bmatrix} P(j\omega) \\ Q(j\omega) \end{bmatrix}^* \Pi(j\omega) \begin{bmatrix} P(j\omega) \\ Q(j\omega) \end{bmatrix} d\omega \geq 0 \tag{1}$$

where $P(j\omega)$ and $Q(j\omega)$ are the Fourier transform of the signals p and q respectively. From [19, Theorem 1], the feedback connection between H, a stable LTI system with bounded infinity norm, and a bounded causal operator $\mathbb{\Delta}$ (see Fig. 1) is stable if,

1) the interconnection of H and $\tau\mathbb{\Delta}$ is well-posed for all $\tau \in [0, 1]$;

2) $\tau\mathbb{\Delta}$ satisfies the IQC defined by Π for all $\tau \in [0,1]$;
3) $\exists\, \epsilon > 0$ such that

$$\begin{bmatrix} H(j\omega) \\ I \end{bmatrix}^* \Pi(j\omega) \begin{bmatrix} H(j\omega) \\ I \end{bmatrix} \prec 0 \qquad \forall \omega \in \Omega \tag{2}$$

Remark 1: If the upper left corner of Π is positive semi-definite and the lower right corner is negative semi-definite, then using [19, Remark 2], $\tau\mathbb{\Delta}$ satisfies the IQC defined by Π for all $\tau \in [0,1]$ if and only if $\mathbb{\Delta}$ satisfies the IQC.

Numerous forms of multiplier matrices $\Pi(j\omega)$ for different uncertainty types have been proposed in literature. For arbitrarily fast time-varying scalar uncertainties, i.e. $\mathbb{\Delta}(k) = \delta(k)I$, $|\delta(k)| \leq \eta, \forall k \in \mathbb{R}_+$, $\Pi(j\omega)$ can be defined as [26]:

$$\Pi(j\omega) = \begin{pmatrix} \eta^2 D(j\omega) & E(j\omega) \\ E(j\omega)^* & -D(j\omega) \end{pmatrix}, \tag{3}$$

where $D = D^* \succeq 0,\ E = -E^*$ are bounded functions of $j\omega$.

A system analysis step can be performed using (1) to find a multiplier matrix $\Pi(j\omega)$ which satisfies the constraint. From (3), the upper bound η on $|\delta(k)|$ can be identified allowing to compute bounds on the uncertainty block $\mathbb{\Delta}(k)$. Similarly, (3) can be used as a control design constraint to guarantee robustness for a desired fixed upper bound η.

B. Basic problem statement

The general objective is to reject external perturbations in the closed-loop. The system to be controlled is a multivariable linear time-invariant (LTI-MIMO) plant P_2 referred to as secondary path with m input channels and n output channels. Its frequency response function (FRF) matrix is the matrix where $\{k,l\}^{\text{th}}$ element is the FRF from the input channel l to the output channel k. The FRF matrix can be acquired from classical system identification experiments [27]. It is assumed that $P_2(j\omega)$ is bounded for all frequencies $\omega \in \Omega$. Given N samples of an input signal u and of an output signal y which can be acquired from an open-loop identification experiment, the corresponding plant FRF can be estimated as:

$$P_2(j\omega) = \left[\sum_{n=0}^{N-1} y(n) e^{-j\omega T_s n}\right] \left[\sum_{n=0}^{N-1} u(n) e^{-j\omega T_s n}\right]^{-1} \tag{4}$$

The estimation errors can be considered as model uncertainty and taken into account for the controller design, however, they are neglected to focus on the main subject of this paper. In addition, a perturbation model $P_1(j\omega)$ representative of the primary path can be used to model the propagation of an exogenous perturbation signal d to the measurement y. No precise knowledge of $P_1(j\omega)$ is required. However, a sinusoidal component with an unknown time-varying harmonic frequency $\rho(k)$ is supposed to be part of $P_1(j\omega)$.

C. Control design for LFT systems

A method to design fixed-structure frequency-domain controller based on linear fractional transform (LFT) representation is presented in [28]. A convex optimisation problem using LMIs is proposed to obtain an LTI controller with a fixed-structure parametrization. Since this method will be used in this paper, a summary of the main result is given in this section.

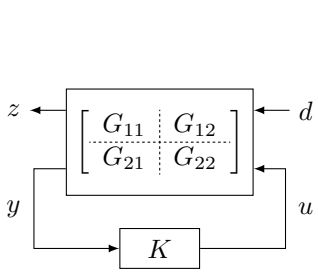

Fig. 2. LFT interconnection between generalized system and controller

The FRF of a generalized system $\mathcal{G}$ with exogenous signals $d \in \mathbb{R}^{n_d}$, control inputs $u \in \mathbb{R}^{n_u}$, measurements $y \in \mathbb{R}^{n_y}$ and performance channels $z \in \mathbb{R}^{n_z}$ can be presented as:

$$\begin{bmatrix} z \\ y \end{bmatrix} = \left[\begin{array}{c|c} G_{11} & G_{12} \\ \hline G_{21} & G_{22} \end{array}\right] \begin{bmatrix} d \\ u \end{bmatrix}.$$

The aim is to design an LTI controller K in order to compensate for the effect of the exogenous disturbances d on the performance channels z. The corresponding LFT represented in Fig. 2 is given by

$$T_{zd} = G_{11} + G_{12}K(I - G_{22}K)^{-1}G_{21}. \tag{5}$$

Assuming the closed-loop system is stable, the infinity norm of T_{zd} can be expressed as

$$||T_{zd}||_\infty^2 = \sup_{\omega\in\Omega} \bar{\sigma}(T_{zd}^*(j\omega)T_{zd}(j\omega))$$

where $\bar{\sigma}$ is the maximum singular value. This can be evaluated if $G(j\omega)$, the FRF of $\mathcal{G}$, $\forall \omega \in \Omega$ is available. The controller design problem, in this case, can be formulated as the minimization of the spectral norm:

$$\begin{aligned} &\min_{K,\gamma} \gamma \\ &\text{s.t.} \quad T_{zd}^*(j\omega)T_{zd}(j\omega) \preceq \gamma I, \qquad \forall \omega \in \Omega \end{aligned} \tag{6}$$

The controller K can be parameterized as $K = Y^{-1}X$, where X and Y are both $\mathcal{RH}_\infty$ matrix functions linear in optimization variables. Assuming that G_{12} is full column rank $\forall \omega \in \Omega$, we can define

$$\Phi = (Y - XG_{22})\, G_{12}^{\mathsf{L}},$$

as a linear function of the optimization variables. Then, T_{zd} can be expressed as

$$T_{zd} \quad = \Phi^{\mathsf{R}} (\Phi G_{11} + XG_{21}) + \Psi G_{11} \tag{7}$$

where $\Psi = I - \Phi^{\mathsf{R}}\Phi = I - G_{12}G_{12}^{\mathsf{L}}$. The constraint from (6) can now be reformulated as,

$$\begin{aligned} T_{zd}^* T_{zd} = {} & (\Phi G_{11} + XG_{21})^* (\Phi\Phi^*)^{-1} (\Phi G_{11} + XG_{21}) \\ & + (\Psi G_{11})^* (\Psi G_{11}) \prec \gamma I \end{aligned} \tag{8}$$

using the fact that $\Psi^*\Phi^{\mathsf{R}} = \Psi\Phi^{\mathsf{R}} = \Phi^{\mathsf{R}} - \Phi^{\mathsf{R}}\Phi\Phi^{\mathsf{R}} = \mathbf{0}$ and $(\Phi\Phi^*)^{\mathsf{R}} = (\Phi\Phi^*)^{-1}$. Using the Schur complement lemma, (8) can be expressed as

$$\begin{bmatrix} \gamma I - \Lambda & (\Phi G_{11} + XG_{21})^* \\ (\Phi G_{11} + XG_{21}) & \Phi\Phi^* \end{bmatrix} \succ \mathbf{0}, \tag{9}$$

where $\Lambda = (\Psi G_{11})^*(\Psi G_{11})$. This constraint is not convex and does not guarantee the closed-loop stability. It is shown

in [28] that a convex lower-bound on the quadratic term $\Phi\Phi^*$ can be obtained that ensure the closed-loop stability as well:

$$\Phi\Phi^* \succeq \Phi\Phi_c^* + \Phi_c\Phi^* - \Phi_c\Phi_c^* \tag{10}$$

where $\Phi_c = (Y_c - X_c G_{22})\, G_{12}^{\mathsf{L}}$, and $K_c = Y_c^{-1} X_c$ is an initial stabilizing controller. This leads to:

$$\begin{aligned} &\min_{X,Y} \gamma \\ &\begin{bmatrix} \gamma I - \Lambda & (\Phi G_{11} + X G_{21})^* \\ \star & \Phi\Phi_c^* + \Phi_c\Phi^* - \Phi_c\Phi_c^* \end{bmatrix} (j\omega) \succ \mathbf{0} \quad \forall \omega \in \Omega, \end{aligned} \tag{11}$$

To solve the optimisation problem, a grid-based approach can be employed. The results can be improved using an iterative approach where the controller K is used as the initial stabilising control for the next iteration. This sequence of convex optimisation problems converges to a local optimal solution of the original nonlinear problem. For a more detailed explanation of the method, refer to [28].

III. Main Results

A. Controller structure for single harmonic rejection

Due to the time-varying nature of the disturbance frequency, P_2 shall be controlled by an LPV controller. We choose the LPV controller as the multiplication of an LTI controller $K(z)$ and an inverted time-varying filter $N(z, \theta(k))$:

$$K_N(z, \theta(k)) = K(z) N(z, \theta(k)),$$

where $\theta(k) \in \Theta$ is the scheduling parameter. The control system architecture is schematically presented in Fig. 3. The time-varying notch filter $N(z, \theta(k))$ ensures asymptotic performance for the disturbance rejection, in accordance to the IMP. This part of the control system is defined as:

$$N(z, \theta(k)) = \frac{\alpha}{1 + \beta\theta(k) z^{-1} + \beta^2 z^{-2}}, \tag{12}$$

where α and β are scalar factors allowing to adjust gain and damping of the inverted notch filter and $\theta(k) = -2\cos(T_s \rho(k))$ where $\rho(k)$ is the time-varying central frequency of the notch and T_s the sampling period of the controller.

The time-invariant part of the controller is parameterised by $K(z) = Y(z)^{-1} X(z)$ and is computed by a convex optimisation problem to guarantee closed-loop stability for all the variations in the scheduling parameter $\theta(k)$. A sliding discrete Fourier transform (SDFT) is used for the estimation of the unknown harmonic disturbance frequency (see Section IV-B). The scheduling parameter $\theta(k)$ can be defined around a fixed central notch frequency $\bar{\theta}$ as $\theta(k) = \bar{\theta} + \delta\theta(k)$ with $|\delta\theta(k)| \leq \eta$ such that $[\theta_{\min}, \theta_{\max}] = [\bar{\theta} - \eta, \bar{\theta} + \eta]$. $\theta(k)$ is a time-varying parameter allowing to modify the notch frequency according to the estimated harmonic frequency. The objective is to guarantee the closed-loop stability when $\theta(k)$ is varying.

B. Generalized model as LFR

In the first step, we "pull out" $\delta\theta(k)$ from $N(z, \theta(k))$ and form a multivariable time-varying block $\Delta(k)$ describing the time-varying nature of $\theta(k)$. The parametrization of

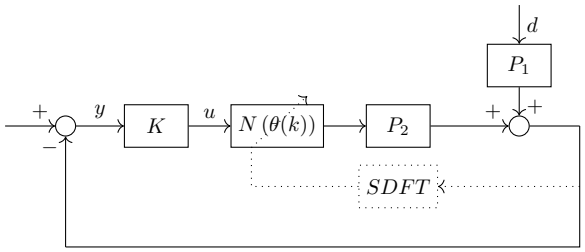

Fig. 3. Control system architecture with LTI controller part

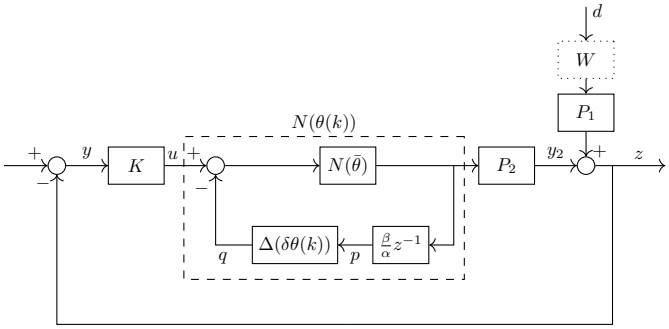

Fig. 4. Closed-loop scheme with $N(z, \theta(k))$ represented as a feedback loop to "pull out" $\Delta(\delta\theta(k))$

$N(z, \theta(k))$ allows an equivalent representation as a feedback loop as shown in Section III-B:

$$\begin{aligned} N(z, \theta(k)) &= \frac{\alpha}{1 + \beta\theta(k) z^{-1} + \beta^2 z^{-2}} \\ &= \frac{\frac{\alpha}{1 + \beta\bar{\theta} z^{-1} + \beta^2 z^{-2}}}{1 + \frac{\beta z^{-1}}{1 + \beta\bar{\theta} z^{-1} + \beta^2 z^{-2}} \delta\theta(k)} \\ &= \frac{N(z, \bar{\theta})}{1 + \frac{\beta}{\alpha} z^{-1} N(z, \bar{\theta}) \delta\theta(k)} \end{aligned}$$

In the second step, the LTI plant model P_2 will be augmented with $N(z, \theta(k))$ and will be represented by an LFR. The augmented plant G^s maps q (output of $\Delta(k)$) and the control inputs u to p (input of $\Delta(k)$) and to y_2 (the output of P_2). This augmented plant does not include the disturbance d and will be used to define a convex set of stabilizing controllers.

From Section III-B, G^s can be extracted by expressing the connections between u, p, q and y_2, and is given by

$$\begin{aligned} \begin{pmatrix} p \\ y_2 \end{pmatrix} &= \begin{pmatrix} G_{11}^s & G_{12}^s \\ G_{21}^s & G_{22}^s \end{pmatrix} \begin{pmatrix} q \\ u \end{pmatrix} \\ &= \begin{pmatrix} -\frac{\beta}{\alpha} z^{-1} N(\bar{\theta}) & \frac{\beta}{\alpha} z^{-1} N(\bar{\theta}) \\ -P_2 N(\bar{\theta}) & P_2 N(\bar{\theta}) \end{pmatrix} \begin{pmatrix} q \\ u \end{pmatrix}, \end{aligned} \tag{13}$$

and $\Delta(k) \in \mathbb{R}^{n_u \times n_u}$ is parameterised as

$$q = \Delta(k)\ p = \delta\theta(k) I\ p \tag{14}$$

The scheme representing the augmented system is given in Fig. 5. A relation between the non-parametric LFT $T_{pq}(j\omega)$ and $\Delta(k)$ can now be represented in the form of an IQC allowing to establish a closed-loop stability guarantee for the arbitrarily fast variation of $\theta(k)$. The details of the development are presented in Section III-C.

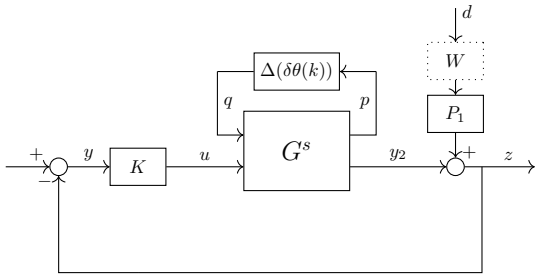

Fig. 5. Closed-loop scheme with the augmented system

Note that the time-varying inverted notch filter ensures asymptotic attenuation of the disturbances. However, the nominal transient performance can also be defined and optimized using an additional LFR for $T_{zd}(j\omega)$ to minimize the effect of the external perturbation signal d on the performance channel z (see Section III-B). The corresponding augmented plant G^p is given by

$$\begin{pmatrix} z \\ y \end{pmatrix} = \begin{pmatrix} G^p_{11} & G^p_{12} \\ G^p_{21} & G^p_{22} \end{pmatrix} \begin{pmatrix} d \\ u \end{pmatrix} \tag{15}$$

$$= \begin{pmatrix} P_1 W & P_2 N(\bar{\theta}) \\ -P_1 W & -P_2 N(\bar{\theta}) \end{pmatrix} \begin{pmatrix} d \\ u \end{pmatrix}, \tag{16}$$

where W is a weighting filter which can be chosen according to the performance objective. It may typically be chosen as $W(j\omega) = N(j\omega, \bar{\theta})$.

C. Controller Design

The stability for arbitrarily fast time-varying scheduling parameter shall be guaranteed using an IQC-based constraint.

A simplified solution for Π in accordance to (3), choosing $D = I$ and $E = 0$, is given by

$$\Pi = \begin{pmatrix} \eta^2 I & 0 \\ 0 & -I \end{pmatrix}. \tag{17}$$

When inserting (17) in (2), the obtained inequality can be simplified:

$$\begin{bmatrix} T_{pq}(j\omega) \\ I \end{bmatrix}^* \begin{pmatrix} \eta^2 I & 0 \\ 0 & -I \end{pmatrix} \begin{bmatrix} T_{pq}(j\omega) \\ I \end{bmatrix} \prec 0 \qquad \forall \omega \in \Omega$$

$$\Leftrightarrow \quad T^*_{pq}(j\omega) T_{pq}(j\omega) \prec \eta^{-2} I \qquad \forall \omega \in \Omega \tag{18}$$

This inequality has the same form as the constraint in (6) and can be converted to a set of LMIs in the same way as for the general LFT systems presented in Section II-C and be integrated to the optimization problem in (6) as follows:

$$\begin{aligned} & \min_{K,\gamma} \gamma \\ \text{s.t.} \quad & T^*_{zd}(j\omega) T_{zd}(j\omega) \preceq \gamma I, \qquad \forall \omega \in \Omega \\ & T^*_{pq}(j\omega) T_{pq}(j\omega) \prec \eta^{-2} I, \quad \forall \omega \in \Omega \end{aligned} \tag{19}$$

An alternative approach involves fixing γ and maximizing η for robustness or minimizing γ while simultaneously maximizing η by a multi-objective optimization. However, a trade-off between the two objectives needs a weighting factor which is difficult to tune. Therefore, a two-step optimization algorithm is proposed. In the first step, a controller K is computed to minimize γ while keeping η fixed. In the second step, the optimal controller K and γ are fixed and η is maximized under the constraint described in (18). This step involves a convex problem with respect to η^{-2} and there is no need to approximate the quadratic term $\Phi\Phi^*$. To improve the obtained control performance, this two-step process is iterated until η_i no longer increases in iteration i. The procedure to obtain the desired LPV controller is summerized in Algorithm 1 where a frequency grid is used as $\Omega_N = \{\omega_1, \ldots, \omega_N\}$.

Algorithm 1 Two-step iterative LPV control design

Require: $\epsilon > 0$

$\eta_1 \leftarrow \epsilon$

while $\eta_i - \eta_{i-1} > \epsilon$ **do**

- Solve for optimal X°, Y° and γ°

$$\min_{X,Y,\gamma} \quad \gamma$$

$$\text{s.t.} \quad \begin{pmatrix} \gamma I - \Lambda & (\Phi^p G^p_{11} + X G^p_{21})^* \\ \star & \Phi^p (\Phi^p_c)^* + \Phi^p_c (\Phi^p)^* - \Phi^p_c (\Phi^p_c)^* \end{pmatrix} \succ 0,$$

$$\begin{pmatrix} \eta_i^{-2} I - \Lambda & (\Phi G^s_{11} + X G^s_{21})^* \\ \star & \Phi^s (\Phi^s_c)^* + \Phi^s_c (\Phi^s)^* - \Phi^s_c (\Phi^s_c)^* \end{pmatrix} \succ 0$$

$\forall \omega \in \Omega_N$

where $\Phi^p = (Y - X G^p_{22}) (G^p_{12})^{\mathsf{L}}$,

$\Phi^s = (Y + X G^s_{22}) (G^s_{12})^{\mathsf{L}}$

- Solve for η_i

$$\min_{\eta_i} \quad \eta_i$$

$$\text{s. t.} \quad \begin{pmatrix} \eta_i^{-2} I - \Lambda & (\Phi^\circ G^s_{11} + X^\circ G^s_{21})^* \\ \star & \Phi^\circ (\Phi^\circ)^* \end{pmatrix} \succ 0,$$

$\Phi^\circ = (Y^\circ + X^\circ G^s_{22}) (G^s_{12})^{\mathsf{L}}$

$\forall \omega \in \Omega_N$

- Increment i

end while

The choice of Π as presented in (17) is conservative because the off-diagonal terms are set to zero and Π is not a function of ω. Hence, the actual η_n in the last iteration n is somewhat larger then the value computed with Algorithm 1. The conservatism can be reduced using a full parameterized Π given by

$$\Pi(j\omega) = \begin{pmatrix} \Pi_{11}(j\omega) & \Pi_{12}(j\omega) \\ \Pi^*_{12}(j\omega) & \Pi_{22}(j\omega) \end{pmatrix}.$$

Algorithm 2 can be used after the completion of Algorithm 1 to obtain a stability guarantee for an interval bound $\eta_{\max}$ which is larger than η_n obtained from the Algorithm 1 after n iterations. Algorithm 2 can be solved using a bisection approach or by iteratively increasing the value of $\eta_{\max}$ and checking the

problem's feasibility. The multiplier matrix Π could be taken invariant with respect to ω. This reduces significantly the computational complexity while the achieved $\eta_{\max}$ may not increase significantly.

Algorithm 2 Stability analysis of final controller

$$\begin{aligned}
&\max_{\Pi,\eta_{\max}} \quad \eta_{\max} \\
\text{s.t. } &\begin{bmatrix} T_{pq}(j\omega) \\ I \end{bmatrix}^* \Pi(j\omega) \begin{bmatrix} T_{pq}^*(j\omega) \\ I \end{bmatrix} \prec 0 \qquad \forall \omega \in \Omega_N, \\
&\begin{bmatrix} I \\ \eta_{\max} I \end{bmatrix}^* \Pi(j\omega) \begin{bmatrix} I \\ \eta_{\max} I \end{bmatrix} \succ 0, \qquad \forall \omega \in \Omega_N, \\
&\Pi_{11}(j\omega) \succ 0, \quad \Pi_{22}(j\omega) \prec 0 \qquad \forall \omega \in \Omega_N,
\end{aligned}$$

D. Controller structure for multi-harmonic rejection

In presence of a sinusoidal perturbation signal containing n harmonic frequencies $\rho(k) = [\rho_1, \rho_2, ..., \rho_n]$, a sequence of inverted notch filters stacked in series can be defined as:

$$N\left(z, \theta_1(k), ..., \theta_n(k)\right) = \prod_{i=1}^{n} \frac{\alpha}{1 + \beta\theta_i(k) z^{-1} + \beta^2 z^{-2}}, \quad (21)$$

where $\theta_i(k) = -2\cos\left(T_s \rho_i(k)\right)$.

$\Delta(k) \in \mathbb{R}^{n_u n \times n_u n}$ is parameterised as

$$q = \Delta(k)\ p = \begin{pmatrix} \eta_1 I & \mathbf{0} & \mathbf{0} & \mathbf{0} \\ \mathbf{0} & \eta_2 I & \mathbf{0} & \mathbf{0} \\ & & \ddots & \mathbf{0} \\ \mathbf{0} & \mathbf{0} & \mathbf{0} & \eta_n I \end{pmatrix} p \quad (22)$$

Similar to the development of (13), $N\left(\theta_1(k), ..., \theta_n(k)\right)$ can be represented as a feedback connection as shown in Fig. 6 and a generalized plant $G_n^p(j\omega)$ can be computed (see Eq. 20) by defining $\theta_i(k) = \bar{\theta}_i + \delta\theta_i(k)$.

IV. Experimental Results

A. Hybrid micro-vibration damping platform (MIVIDA)

Novel high-precision optical instruments designed for Earth observation missions demand an exceptionally high pointing accuracy. These line-of-sight stability requirements constrain the admissible level of mechanical vibration that can occur onboard a spacecraft. Micro-vibrations are caused by primary satellite systems such as reaction wheels, thrusters, cryocoolers, or solar array drive mechanisms, and have the potential to significantly degrade the performance of the sensitive payloads.

A hybrid active-passive micro-vibration damping platform (MIVIDA), aimed at mitigating micro-vibrations and isolating the sensitive optical payload from external disturbances, was developed at CSEM. The objective is to study in a more general context the stabilisation of sensitive active payloads from multiple unknown external perturbations. The modular platform consists of an adjustable number of passive dampers, a set of proof mass actuators (PMA) creating a 6 degree of freedom (DoF) force tensor, and a payload interface allowing to accommodate various types of sensitive instruments. The platform utilises accelerometer measurements in close proximity to the payload to actively reject disturbances from the satellite body. These external perturbations are generated using an external inertial shaker. An image of the system is shown in Fig. 7. All experimental tests with the platform are carried out at the Microvibration Characterisation Facility at CSEM in Neuchâtel, Switzerland [29].

B. Scheduling parameter update

The scheduling parameter is updated by estimating the main harmonic frequency of the perturbation. As the perturbation signal d cannot be measured directly, an estimation of the harmonic frequency is calculated based on a sliding discrete Fourier transform (SDFT) on the output signal y. The SDFT is implemented using the algorithm presented in [30]. The discrete Fourier transform (DFT) is given by

$$X(k) = \sum_{n=0}^{N-1} x(n) e^{-j2\pi k n/N}$$

The DFT can be computed recursively using the SDFT algorithm. Essentially, the SDFT algorithm arises from the fact that for two successive times $n-1$ and n, the sequences $x(n-1)$ and $x(n)$ contain mainly identical elements. The recursive update step of the SDFT can be expressed by

$$X_k(n) = \big(X_k(n-1) - x(n-N) + x(n)\big) e^{(j2\pi k/N)}.$$

$$\begin{pmatrix} p_1 \\ \vdots \\ p_i \\ \vdots \\ p_n \\ y \end{pmatrix} = \begin{pmatrix} -\frac{\beta}{\alpha} z^{-1} N(\bar{\theta}_1) & & \mathbf{0}_{1\times(n-1)} & & \frac{\beta}{\alpha} z^{-1} N(\bar{\theta}_1) \\ & & \vdots & & \\ -\frac{\beta^i}{\alpha} z^{-1} \prod_{j=1}^{i} N(\bar{\theta}_j) & \dots & -\frac{\beta^i}{\alpha} z^{-1} N(\bar{\theta}_i) & \mathbf{0}_{1\times(n-i)} & \frac{\beta^i}{\alpha} z^{-1} \prod_{j=1}^{i} N(\bar{\theta}_j) \\ & & \vdots & & \\ -\frac{\beta^n}{\alpha} z^{-1} \prod_{j=1}^{n} N(\bar{\theta}_j) & \dots & & -\frac{\beta^n}{\alpha} z^{-1} N(\bar{\theta}_n) & \frac{\beta^n}{\alpha} z^{-1} \prod_{j=1}^{n} N(\bar{\theta}_j) \\ P_2 \prod_{j=1}^{n} N(\bar{\theta}_j) & \dots & & P_2 N(\bar{\theta}_n) & -P_2 \prod_{j=1}^{n} N(\bar{\theta}_j) \end{pmatrix} (j\omega) \begin{pmatrix} q_1 \\ \vdots \\ q_i \\ \vdots \\ q_n \\ u \end{pmatrix}, \quad (20)$$

$$u = Ky$$

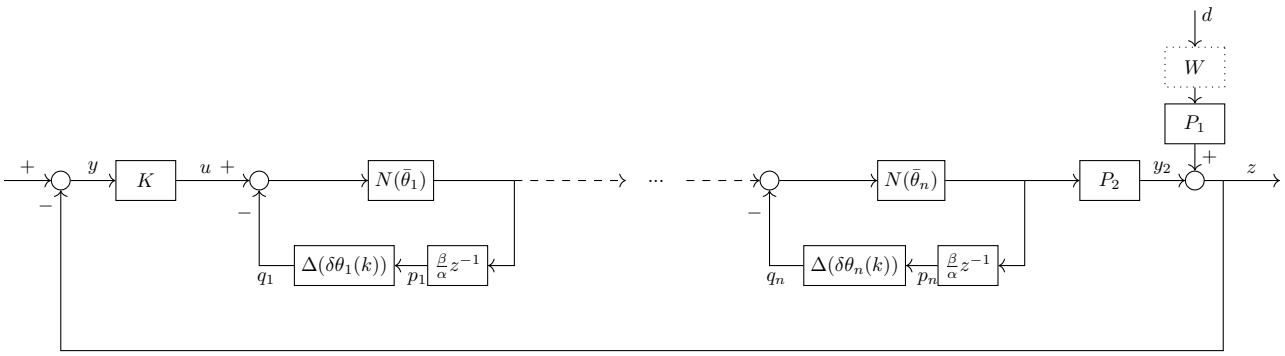

Fig. 6. Control scheme with $N\left(\theta_1(k), ..., \theta_n(k)\right)$ represented as a feedback loop for the multi-harmonic case

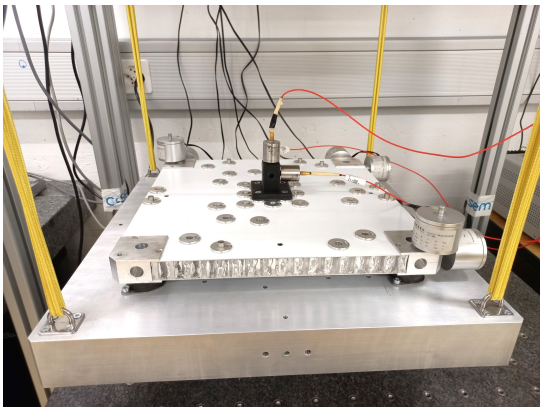

Fig. 7. Hybrid micro-vibration damping platform MIVIDA developed at CSEM, Switzerland

	Attenuation Performance (dB)		
	X-axis	Y-axis	Z-axis
$\rho(k) = \bar{\rho} = 60$ Hz	20.03	15.67	15.22
$\rho(k) = \bar{\rho} - \delta\rho_{\max} =$ 44 Hz	21.70	26.36	6.12
$\rho(k) = \bar{\rho} + \delta\rho_{\max} =$ 76 Hz	16.30	-0.31	14.22

TABLE I
ATTENUATION PERFORMANCE ACHIEVED WITH THE IQC-BASED LPV CONTROLLER AT DIFFERENT VALUES OF $\rho(k)$

C. Single harmonic rejection validation on MIVIDA

The here presented method is used to design a controller for the MIVIDA platform allowing to adaptively reject sinusoidal disturbances. A system identification experiment is carried out to compute an FRF matrix directly from experimental data using a frequency grid with 1000 points and a sampling frequency of 1 kHz. For the control design, a center frequency $\bar{\rho}$ of 60 Hz and ϵ of 1 Hz is used. The tuning parameters of $N(z, \theta(k))$ are chosen $\alpha = 0.1$ and $\beta = 0.997$. The identified FRF matrix $P_2(j\omega)$ together with the computed sensitivity function $S(j\omega)$ are presented in Fig. 8. It can be observed that the disturbance frequency is attenuated about 30 dB along the three axes. For the primary path, no identification experiment was performed and $P_1(j\omega) = I$ is taken for simplicity and for generality of the problem. The obtained controller guarantees stability for a value of $\delta\rho_{\max} = 15.78$ Hz. This is the resulting value obtained with Algorithm 2 using a Π which is invariant with respect to ω. When computing a $\Pi(j\omega)$, the achieved $\delta\rho_{\max}$ differs only in the order of 10^{-3} compared to the invariant Π while the computational complexity is significantly higher. The value obtained after the last iteration with Algorithm 1 is $\delta\rho_{\max} = 10.72$ Hz.

A dSpace rapid prototyping platform is used as real-time control system at a sampling frequency of 1 kHz. Two individual power amplifiers generate the power supply and the analog input and output signals for the PMA and the accelerometers respectively. A third control module is used for the command of the external inertial shaker. For performance evaluation, a sinusoidal perturbation along the x-axis is injected with this shaker. In Fig. 9, the measured accelerations along the three axes in open- and closed-loop are shown. The harmonic frequency $\rho(k)$ of the sinusoidal perturbation is shifted in the interval of $\rho(k) \in [44, 76]$ Hz increasing the frequency by 2 Hz every 5 seconds. Table 1 shows the obtained attenuation values for different values of $\rho(k)$. The difference between the attenuation computed using the sensitivity function and the experimental results comes from the magnitude of the primary path model $P_1(j\omega)$ at the disturbance frequencies. Furthermore, the actual limit of stability when increasing the value of $\delta\rho_{\max}$ was assessed. When injecting a sinusoidal perturbation with $\rho(k) = 37$ Hz, the closed-loop system becomes unstable. Hence, there is some margin in the stability limit determined at $\delta\rho_{\max} = 15.78$ Hz while the experimentally determined value is at approximately $\delta\rho_{\max} = 22$ Hz.

An additional test has been performed to assess the closed-loop stability for a fast variation of the scheduling parameters. During that test, the harmonic frequency $\rho(k)$ of the sinusoidal perturbation is increased by 1 Hz every 100 milliseconds in the interval of $\rho(k) \in [44, 76]$. From Fig. 10, it can be observed that the stability is still guaranteed in closed-loop. Note that the attenuation performance cannot be achieved in that case as the estimation of the disturbance frequency leads to wrong results. The update period of the SDFT needs to be at least 300 miliseconds to obtain a correct estimation. However, the stability of the closed-loop is still guaranteed even if the

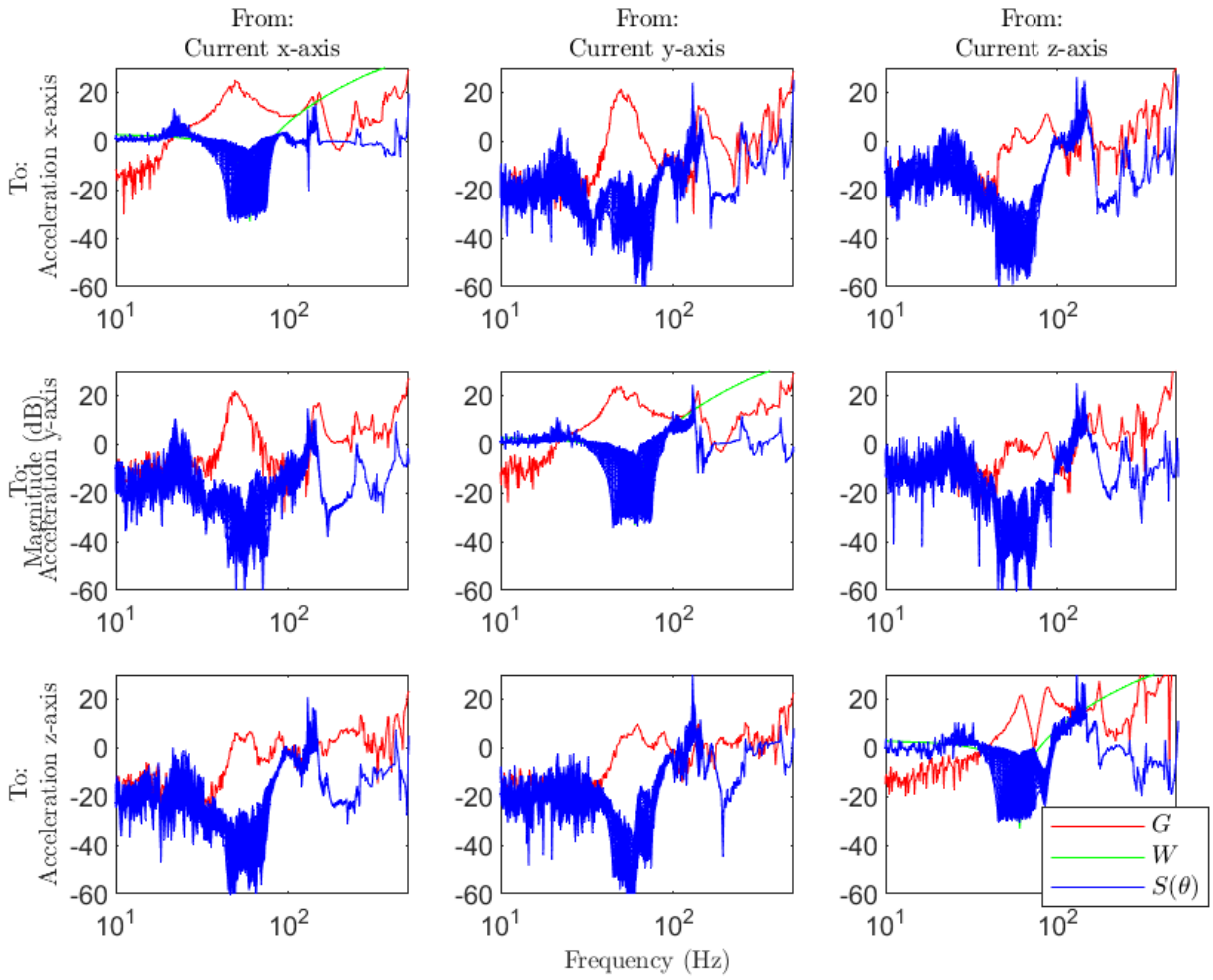

Fig. 8. Closed-loop sensitivity functions $S(\theta)$, FRF matrix of plant model P_2 and performance weighting filter W

estimated disturbance frequency has a large error with respect to the true one.

D. Multi-harmonic rejection validation on MIVIDA

Using the method presented in Section III-D, a controller containing two notch filters $N(z, \theta_1(k), \theta_2(k))$ in series was computed to be applied on MIVIDA. The center frequency $\bar{\rho}_1$ is chosen at 50 Hz and $\bar{\rho}_2 = 70$ Hz with $\epsilon = 0.1$ Hz. The obtained controller guarantees stability for a value of $\delta\rho_{\max} = 5$ Hz. A test injecting a sinusoidal perturbation containing two harmonics was performed. The resulting attenuation performance is presented in Table IV-D. A disturbance attenuation of up to 22.98 dB can be achieved for the central frequency $\bar{\rho}_1$. However, the achieved performance is significantly smaller for other values of $\bar{\rho}_1$ and $\bar{\rho}_2$ and for other axes. When looking at P_2 (see Fig. 8), one can see that the overall magnitude at $\bar{\rho}_2$ is smaller compared to the one at $\bar{\rho}_1$. The signal-to-noise ratio of the accelerometers is therefore smaller at $\bar{\rho}_2$ leading to smaller attenuation performances at higher frequencies. Furthermore, with the given controller structure it is difficult to achieve acceptable performance for multiharmonic rejection due to the parametrization of $N(z, \theta(k))$ with its limited damping adjustment possibilities and due to the waterbed effect. To improve the attenuation performance, a more flexible LPV control structure $K(\theta)$ without fixed parametrization $N(z, \theta(k))$ can be used. In addition, it is possible to use a full parametrized Π as given by (3) also for control synthesis. Such a development is part of on-going work.

		Attenuation Performance (dB)		
First harmonic frequency (Hz)	Second harmonic frequency (Hz)	X-axis	Y-axis	Z-axis
50		7.27	11.12	22.98
	70	3.41	3.82	3.48
52		6.16	10.46	15.49
	68	2.00	1.44	2.28
55		9.12	14.44	9.42
	65	-0.15	-1.19	2.87
53		4.60	4.49	15.82
	67	-1.31	-0.04	-1.34

TABLE II
ATTENUATION PERFORMANCE ACHIEVED WITH THE LPV CONTROLLER FOR DOUBLE HARMONIC REJECTION

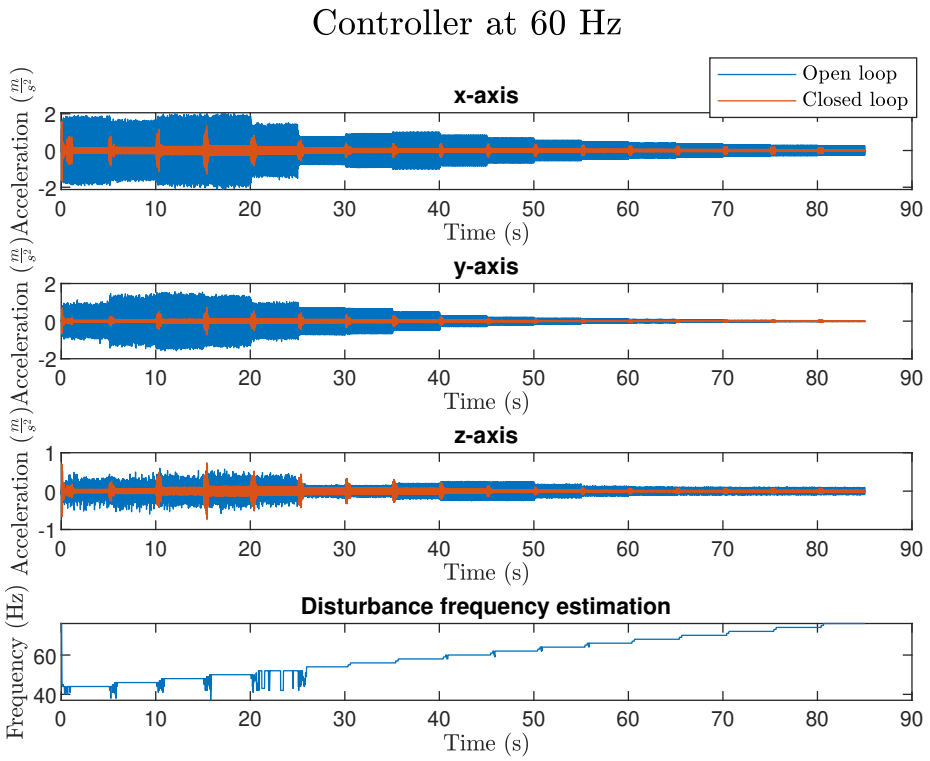

Fig. 9. Closed-loop attenuation test

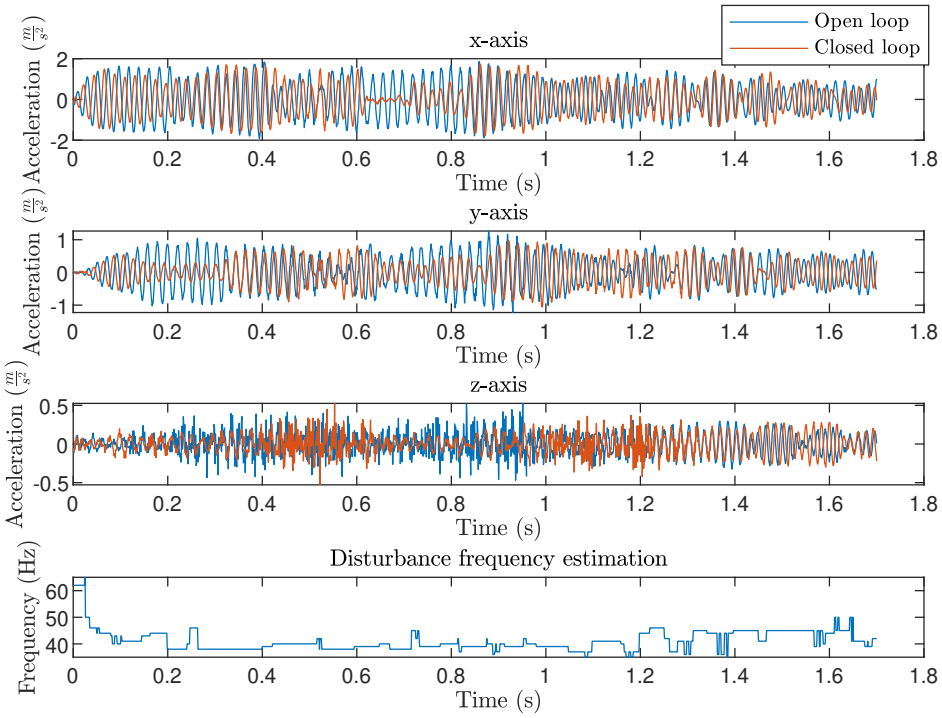

Fig. 10. Fast parameter variation test

V. Conclusions

Given an FRF matrix of an LTI-MIMO system, an LPV controller is computed for adaptive rejection of an unknown external perturbation signal. Using an IQC describing a time-varying real scalar, an equivalent LMI is computed which is included in a two-step iterative control design algorithm. This method allows to guarantee the stability of the controller for arbitrarily fast time-varying scheduling parameters lying in a bounded interval. An LPV controller was designed for the hybrid micro-vibration damping platform using the proposed method. The resulting controller achieves a disturbance attenuation of up to 26.36 dB in the case of single harmonic rejection and up to 22.98 dB for multi-harmonic rejection while guaranteeing stability for scheduling parameters with an arbitrarily fast time-variation.

References

[1] H. E. Tseng and D. Hrovat, "State of the art survey: active and semi-active suspension control," *Vehicle System Dynamics*, vol. 53, no. 7, pp. 1034–1062, 2015. [Online]. Available: http://www.tandfonline.com/doi/full/10.1080/00423114.2015.1037313

[2] Q. Zheng, L. Dong, D. H. Lee, and Z. Gao, "Active disturbance rejection control for MEMS gyroscopes," *IEEE Transactions on Control Systems Technology*, 2009.

[3] R. Fareh, S. Khadraoui, M. Y. Abdallah, M. Baziyad, and M. Bettayeb, "Active disturbance rejection control for robotic systems: A review," *Mechatronics*, vol. 80, p. 102671, 2021. [Online]. Available: https://linkinghub.elsevier.com/retrieve/pii/S0957415821001392

[4] V. Nguyen, J. Johnson, and S. Melkote, "Active vibration suppression in robotic milling using optimal control," *International Journal of Machine Tools and Manufacture*, vol. 152, 2020. [Online]. Available: https://linkinghub.elsevier.com/retrieve/pii/S0890695519312623

[5] T.-B. Airimitoaie, I. D. Landau, R. Melendez, and L. Dugard, "Algorithms for adaptive feedforward noise attenuation—a unified approach and experimental evaluation," *IEEE Transactions on Control Systems Technology*, vol. 29, no. 5, pp. 1850–1862, 2021. [Online]. Available: https://ieeexplore.ieee.org/document/9203846/

[6] P. Ballesteros and C. Bohn, "Disturbance rejection through LPV gain-scheduling control with application to active noise cancellation," *IFAC Proceedings Volumes*, vol. 44, no. 1, pp. 7897–7902. [Online]. Available: https://linkinghub.elsevier.com/retrieve/pii/S1474667016448779

[7] C. Bohn, A. Cortabarria, V. Härtel, and K. Kowalczyk, "Disturbance-observer-based active control of engine-induced vibrations in automotive vehicles," in *Smart Structures and Materials 2003: Modeling, Signal Processing, and Control*, R. C. Smith, Ed., vol. 5049, International Society for Optics and Photonics. SPIE, 2003, pp. 565 – 576. [Online]. Available: https://doi.org/10.1117/12.482709

[8] C. Kinney and R. De Callafon, "An adaptive internal model-based controller for periodic disturbance rejection," *IFAC Proceedings Volumes*, vol. 39, no. 1, pp. 273–278. [Online]. Available: https://linkinghub.elsevier.com/retrieve/pii/S1474667015352745

[9] I. D. Landau, A. Castellanos Silva, T.-B. Airimitoaie, G. Buche, and M. Noe¨, "Benchmark on adaptive regulation—rejection of unknown/time-varying multiple narrow band disturbances," vol. 19, no. 4, pp. 237–252. [Online]. Available: https://linkinghub.elsevier.com/retrieve/pii/S0947358013000721

[10] X. Chen and M. Tomizuka, "Selective model inversion and adaptive disturbance observer for rejection of time-varying vibrations on an active suspension," in *2013 European Control Conference (ECC)*. IEEE, pp. 2897–2903. [Online]. Available: https://ieeexplore.ieee.org/document/6669759/

[11] A. Karimi and Z. Emedi, "H-inf gain-scheduled controller design for rejection of time-varying narrow-band disturbances applied to a benchmark problem," *European Journal of Control*, vol. 19, no. 4, pp. 279–288. [Online]. Available: https://linkinghub.elsevier.com/retrieve/pii/S0947358013000757

[12] B. Vau and I. D. Landau, "Adaptive rejection of narrow-band disturbances in the presence of plant uncertainties—a dual youla–kucera approach," *Automatica*, vol. 129, p. 109618. [Online]. Available: https://linkinghub.elsevier.com/retrieve/pii/S0005109821001382

[13] M. Gevers, "Identification for control: From the early achievements to the revival of experiment design*," *European Journal of Control*, vol. 11, no. 4, pp. 335–352. [Online]. Available: https://linkinghub.elsevier.com/retrieve/pii/S0947358005710414

[14] A. Karimi and C. Kammer, "A data-driven approach to robust control of multivariable systems by convex optimization," *Automatica*, vol. 85, pp. 227–233, Nov. 2017.

[15] S. S. Madani and A. Karimi, "Data-Driven Passivity-Based Current Controller Design for Power-Electronic Converters of Traction Systems," in *Proceedings of the IEEE Conference on Decision and Control*, Jeju Island, Republic of Korea, Dec. 2020, pp. 842–847.

[16] S. S. Madani, C. Kammer, and A. Karimi, "Data-Driven Distributed Combined Primary and Secondary Control in Microgrids," *IEEE Transactions on Control Systems Technology*, vol. 29, no. 3, pp. 1340–1347, May 2021.

[17] S. S. Madani and A. Karimi, "Data-driven LPV controller design for islanded microgrids," *IFAC-PapersOnLine*, vol. 54, no. 7, pp. 433–438, 2021. [Online]. Available: https://linkinghub.elsevier.com/retrieve/pii/S2405896321011721

[18] P. Schuchert and A. Karimi, "Frequency-domain data-driven position-dependent controller synthesis for cartesian robots," *IEEE Transactions on Control Systems Technology*, vol. 31, no. 4, pp. 1855–1866, 2023. [Online]. Available: https://ieeexplore.ieee.org/document/10081199/

[19] A. Megretski and A. Rantzer, "System analysis via integral quadratic constraints," *IEEE Transactions on Automatic Control*, vol. 42, no. 6, pp. 819–830, Jun. 1997.

[20] J. Veenman, C. W. Scherer, and H. Köroğlu, "Robust stability and performance analysis based on integral quadratic constraints," *European Journal of Control*, vol. 31, pp. 1–32, Sep. 2016.

[21] S. Michalowsky, C. Scherer, and C. Ebenbauer, "Robust and structure exploiting optimisation algorithms: An integral quadratic constraint approach," *International Journal of Control*, vol. 94, no. 11, pp. 2956–2979, 2021.

[22] J. Veenman, C. W. Scherer, C. Ardura, S. Bennani, V. Preda, and B. Girouart, "IQClab: A new IQC based toolbox for robustness analysis and control design," *IFAC-PapersOnLine*, vol. 54, no. 8, pp. 69–74, Jan. 2021.

[23] A. Koch, J. Berberich, J. Köhler, and F. Allgöwer, "Determining optimal input–output properties: A data-driven approach," *Automatica*, vol. 134, p. 109906, Dec. 2021.

[24] T. Bloemers, T. Oomen, and R. Tóth, "Frequency Response Data-Based LPV Controller Synthesis Applied to a Control Moment Gyroscope," *IEEE Transactions on Control Systems Technology*, vol. 30, no. 6, pp. 2734–2742, Nov. 2022.

[25] T. Bloemers, T. Oomen, and R. Toth, "Frequency Response Data-Driven LPV Controller Synthesis for MIMO Systems," *IEEE Control Systems Letters*, vol. 6, pp. 2264–2269, 2022.

[26] A. Iannelli, P. Seiler, and A. Marcos, "Region of attraction analysis with integral quadratic constraints," *Automatica*, vol. 109, p. 108543, 2019. [Online]. Available: https://linkinghub.elsevier.com/retrieve/pii/S0005109819304042

[27] R. Pintelon and J. Schoukens, *System Identification: A Frequency Domain Approach*, 2nd ed. John Wiley & Sons, Ltd, 2012.

[28] P. Schuchert, V. Gupta, and A. Karimi, "Data-driven fixed-structure frequency-based $\mathcal{H}_2$ and $\mathcal{H}_\infty$ controller design," 2023 (manuscript submitted for publication). [Online]. Available: https://infoscience.epfl.ch/record/301390

[29] E. Onillon, T. Adam, G. B. Gallego, and E. Klauser, "CSEM micro-vibration characterisation facility description and validation," in *European Space Mechanisms and Tribology Symposium (ESMATS)*, Warsaw, Poland, Sep. 2021.

[30] R. Lyons, "dsp tips & tricks - the sliding DFT," *IEEE Signal Processing Magazine*, vol. 20, no. 2, pp. 74–80, 2003. [Online]. Available: http://ieeexplore.ieee.org/document/1184347/